Invited: Spectral Proper Orthogonal Decomposition of uPSP Measurements in Recent NASA Ames Wind Tunnel Test

Jie Li[1], Kenneth R. Lyons[2], E. Lara Lash[2], Nettie H. Roozeboom[2],
Marc A. Shaw-Lecerf[2], David D. Murakami[2], Nicholas W. Califano[1]

[1]Metis Technology Solutions, Inc.
Moffett Field, CA 94035

[2] NASA Ames Research Center
Moffett Field, CA 94035

This paper discusses Spectral Proper Orthogonal Decomposition (SPOD) of the Unsteady Pressure-Sensitive Paint (uPSP) measurements in recent NASA Ames wind tunnel test. The uPSP measurements were collected using Innovative Scientific Solutions, Inc. (ISSI) porous, fast-response pressure-sensitive paint, 40 ISSI four-inch air-cooled Light-Emitting Diodes, and 8 Phantom v2512 high-speed cameras at 10,000 frames per second in the uPSP Launch Vehicle Demonstration Test (LVDT) of the Space Launch System (SLS) vehicle in the 11-by 11-foot transonic test section of the Unitary Plan Wind Tunnel at NASA Ames Research Center in April 2024. SPOD is derived from a space-time proper orthogonal decomposition problem for statistically stationary flows. SPOD modes are determined in the frequency domain. Each SPOD mode oscillates at a single frequency. SPOD can be viewed as an extension of the Discrete Fourier Transform decomposition and the Dynamic Mode Decomposition. In this paper, the outputs of SPOD of the uPSP measurements in the uPSP LVDT are presented and the effectiveness of SPOD in the identification, diagnosis and analysis of the aerodynamic and aeroacoustic phenomena is demonstrated. The unsteady and dynamic property of the pressure field on the surface of the SLS Block 1B crew vehicle is presented with the visualization of the SPOD modes of the uPSP measurements in the tests of a Mach sweep run of the uPSP LVDT. The SPOD outputs were generated with the execution in parallel of a code in Python, with the library of Message Passing Interface for parallel processing, on the NASA Pleiades supercomputer. The work described in this paper is a part of NASA's development of a new state-of-the-art uPSP capability in production wind tunnels. Funding was provided by the NASA Aerosciences Evaluation and Test Capabilities Portfolio Office of Aeronautics Research Mission Directorate.

Nomenclature

AETC	= NASA Aerosciences Evaluation and Test Capabilities Portfolio Office
ARMD	= NASA Aeronautics Research Mission Directorate
ATAT	= Ascent Transient Aerodynamics Test
CSD	= Cross Spectral Density
DFT	= Discrete Fourier Transform
DMD	= Dynamic Mode Decomposition
FFT	= Fast Fourier Transform
ISSI	= Innovative Scientific Solutions, Inc.
LAS	= Launch Abort System
LED	= Light-Emitting Diode
LVDT	= Launch Vehicle Demonstration Test
MPCV	= Multi-Purpose Crew Vehicle
MPI	= Message Passing Interface
NESC	= NASA Engineering and Safety Center

PSD = Power Spectral Density
SLS = Space Launch System
SPL = Sound Pressure Level
SPOD = Spectral Proper Orthogonal Decomposition
SRB = Solid Rocket Booster
UPWT = NASA Unitary Plan Wind Tunnel
uPSP = Unsteady Pressure-Sensitive Paint
USA = Universal Stage Adapter
$\mathbb{C}$ = set of complex numbers
$\hat{C}_m$ = estimated CSD matrix at the frequency f_m
$f_{binWidth}$ = bin width of DFT, showing the frequency resolution
f_m = frequency corresponding to the vector $\hat{q}_m^{(k)}$
$I_{N_{mode} \times N_{mode}}$ = identity matrix of the dimension $N_{mode} \times N_{mode}$
$\widehat{M}_m$ = Hermitian matrix defined for a computational shortcut to solve for SPOD modes
N_{block} = number of blocks
N_{DFT} = number of frames in a block, i.e., the length of DFT
N_{frame} = number of frames
N_{mode} = number of SPOD modes
N_{node} = number of grid nodes
$N_{overlap}$ = number of overlapped frames
Q = matrix of the full timeseries of uPSP measurements on the grid nodes
$Q^{(k)}$ = matrix of the uPSP measurements in the *k*-th block on the grid nodes, $k = 1, 2, \dots, N_{block}$
$\hat{Q}^{(k)}$ = DFT of the matrix $Q^{(k)}$
$\hat{q}_m^{(k)}$ = *m*-th column of the matrix $\hat{Q}^{(k)}$, $m = 1, 2, \dots, N_{DFT}$
$q_s^{(k)}$ = *s*-th column of the matrix $Q^{(k)}$, $s = 1, 2, \dots, N_{DFT}$
q_t = *t*-th column of the matrix Q, $t = 1, 2, \dots, N_{frame}$
$\mathbb{R}$ = set of real numbers
$\hat{X}_m$ = matrix of the frequency components of the uPSP measurements in all blocks on the grid nodes at the frequency f_m
Λ_m = matrix of eigenvalues of the matrix $\hat{C}_m$
$\lambda_{m,i}$ = *i*-th eigenvalue of the matrix $\hat{C}_m$ arranged in descending order, $i = 1, 2, \dots, N_{mode}$
$\widehat{\Phi}_m$ = matrix of eigenvectors of the matrix $\hat{C}_m$
$\hat{\phi}_{m,i}$ = eigenvector of the matrix $\hat{C}_m$ corresponding to $\lambda_{m,i}$
$\widehat{\Psi}_m$ = matrix of eigenvectors of the matrix $\widehat{M}_m$
$(\cdot)^*$ = conjugate transpose
$\lfloor \cdot \rfloor$ = floor operator

Notice to Readers

Certain features and characteristics of the Space Launch System vehicle are defined by the U.S. Government as Export-Controlled, Controlled Unclassified Information (CUI). To comply with CUI restrictions, values in some plots and figures have been either removed or normalized to arbitrary values. It is the opinion of the authors that these alternations do not detract from the relevant technical discussions.

I. Introduction

This paper discusses Spectral Proper Orthogonal Decomposition (SPOD) of the Unsteady Pressure-Sensitive Paint (uPSP) measurements in recent NASA Ames wind tunnel test (Ref. [1]).

The uPSP measurements were collected using Innovative Scientific Solutions, Inc. (ISSI) Porous, Fast-Response

Pressure-Sensitive Paint (FP-XXX), 40 ISSI four-inch air-cooled Light-Emitting Diodes (LEDs), and 8 Phantom v2512 high-speed cameras at 10,000 frames per second in the uPSP Launch Vehicle Demonstration Test (LVDT) of the Space Launch System (SLS) vehicle in the 11-by 11-foot transonic test section of the Unitary Plan Wind Tunnel (UPWT) at NASA Ames Research Center in April 2024. The models of both the SLS Block 1B crew and cargo configurations were used in the uPSP LVDT. In this paper, only the outputs of SPOD of the uPSP measurements in the tests of the SLS Block 1B crew vehicle are presented. Fig. 1 shows the scale model of the SLS Block 1B crew vehicle installed in the wind tunnel during the uPSP LVDT.

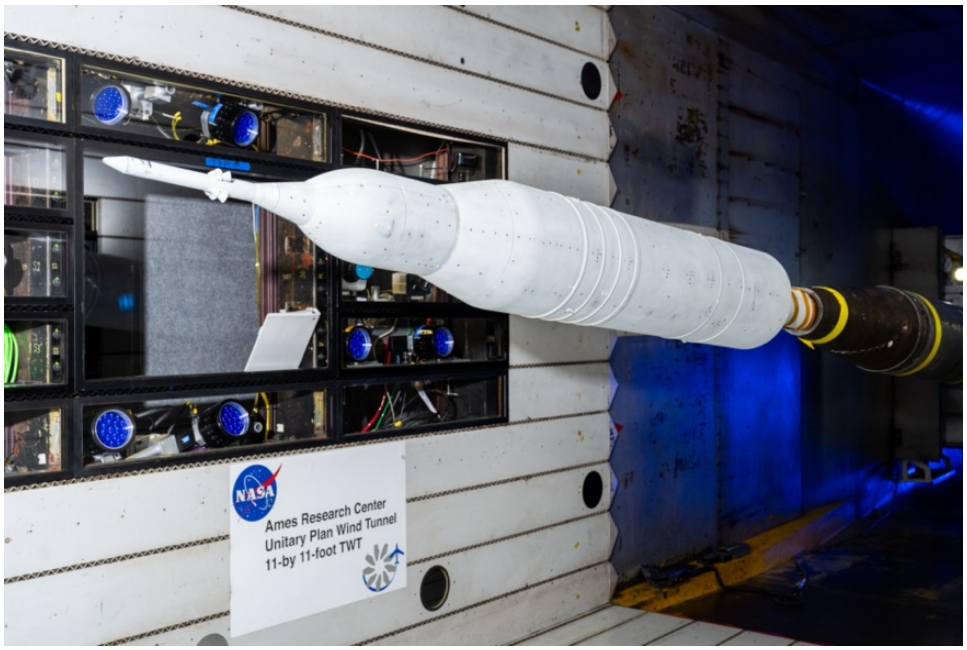

Fig. 1 Scale model of the SLS Block 1B crew vehicle in the 11-by 11-foot transonic test section of the UPWT at NASA Ames Research Center during the uPSP LVDT.

The uPSP measurements, collected with Phantom cameras, were processed with the uPSP data processing software (Ref. [2]). A 7×7 box filter was applied to the raw measurements on the pixels of each camera video frame. The filtered video frames were projected to the grid nodes on the surface of the scale model and converted to engineering units.

SPOD (Refs. [3]-[5]) is derived from a space-time proper orthogonal decomposition problem for statistically stationary flows. SPOD modes are determined in the frequency domain. Each SPOD mode oscillates at a single frequency. SPOD of uPSP measurements consists of two steps: (1) the full timeseries of uPSP measurements are partitioned into a set of smaller, possibly overlapping blocks, and each block is converted from the time domain to the frequency domain with the Discrete Fourier Transform (DFT); (2) at each frequency, the Cross Spectral Density (CSD) matrix is estimated with Welch's method, and the SPOD modes are determined as the eigenvectors of the estimated CSD matrix and arranged in the descending order of the corresponding eigenvalues. SPOD can be viewed as an extension of the DFT decomposition and the Dynamic Mode Decomposition (DMD) (Refs. [6]-[9]).

In this paper, the outputs of SPOD of the uPSP measurements in the uPSP LVDT are presented and the effectiveness of SPOD in the identification, diagnosis and analysis of the aerodynamic and aeroacoustic phenomena is demonstrated. The unsteady and dynamic property of the pressure field on the surface of the SLS Block 1B crew vehicle components, e.g., Launch Abort System (LAS), Multi-Purpose Crew Vehicle (MPCV), Universal Stage Adapter (USA), Core Stage, etc., as shown in Fig. 2, is presented with the visualization of the SPOD modes of the uPSP measurements in the tests of a Mach sweep run of the uPSP LVDT.

The SPOD outputs were generated with the execution in parallel of a code in Python, with the library of Message Passing Interface (MPI) for parallel processing, on the NASA Pleiades supercomputer (Ref. [10]). The code makes use of the open-source packages *SPOD* (Refs. [4], [11]) in MATLAB and *PySPOD* (Ref. [12]) in Python.

The work described in this paper is a part of NASA's development of a new state-of-the-art uPSP capability in production wind tunnels (Refs. [13]-[22]). Funding was provided by the NASA Aerosciences Evaluation and Test Capabilities (AETC) Portfolio Office of Aeronautics Research Mission Directorate (ARMD).

This paper is organized as follows. In Section II, the SPOD algorithm is described. In Section III, the parameters of SPOD of the uPSP measurements are discussed and the outputs of SPOD of the uPSP measurements in the Mach sweep run tests of the uPSP LVDT are presented and discussed. Finally, the conclusions are presented in Section IV.

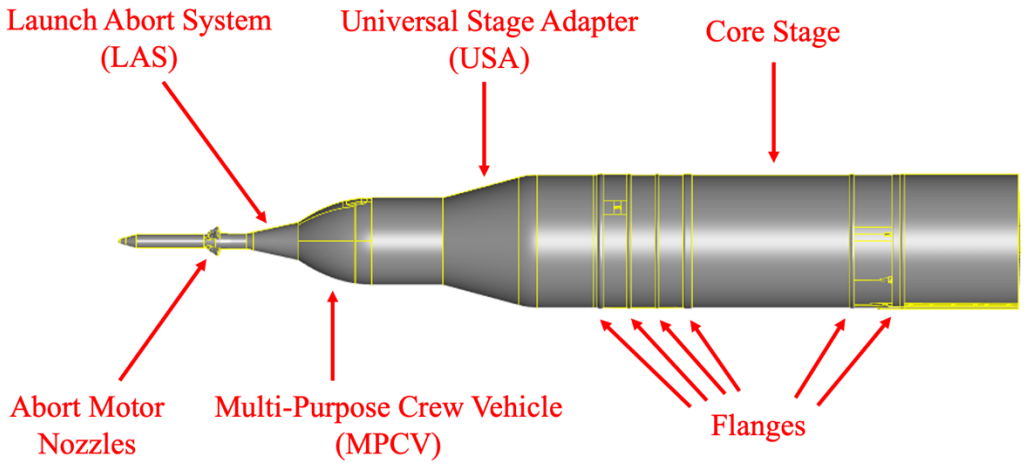

Fig. 2 Components of the SLS Block 1B crew vehicle

II. SPOD Algorithm

In this section, we briefly describe the algorithm to generate the outputs of SPOD of the uPSP measurements presented in Section III. More detailed descriptions of the SPOD algorithm are given in Refs. [3]-[5].

A. DFT of Data in Blocks

Let N_{node} be the number of grid nodes and N_{frame} be the number of frames, the full timeseries of uPSP measurements on the grid nodes can be written as an $N_{node} \times N_{frame}$ matrix of real numbers

$$Q = [q_1 \quad q_2 \quad \cdots \quad q_t \quad \cdots \quad q_{N_{frame}}] \tag{1}$$

where $Q \in \mathbb{R}^{N_{node} \times N_{frame}}$, $q_t \in \mathbb{R}^{N_{node}}$, $t = 1, 2, \ldots, N_{frame}$. $\mathbb{R}$ is the set of real numbers.

The SPOD algorithm consists of two steps. In the first step, the full timeseries of the uPSP measurements are partitioned into a set of smaller, possibly overlapping blocks. Let N_{DFT} be the number of frames in a block, i.e., the length of DFT, and $N_{overlap}$ be the number of overlapped frames, the number of blocks, denoted as N_{block}, is determined as

$$N_{block} = \left\lfloor (N_{frame} - N_{overlap}) / (N_{DFT} - N_{overlap}) \right\rfloor \tag{2}$$

where $\lfloor \cdot \rfloor$ denotes the floor operator.

The uPSP measurements in the k-th block are written as an $N_{node} \times N_{DFT}$ matrix of real numbers

$$Q^{(k)} = \begin{bmatrix} q_1^{(k)} & q_2^{(k)} & \cdots & q_s^{(k)} & \cdots & q_{N_{DFT}}^{(k)} \end{bmatrix} \tag{3}$$

where $Q^{(k)} \in \mathbb{R}^{N_{node} \times N_{DFT}}$, $q_s^{(k)} \in \mathbb{R}^{N_{node}}$, $k = 1, 2, \ldots, N_{block}$, $s = 1, 2, \ldots, N_{DFT}$. It is assumed the mean has been subtracted from the timeseries of the uPSP measurement at each of the grid nodes in a block. The matrix $Q^{(k)}$ of the uPSP measurements in the k-th block is converted from the time domain to the frequency domain with the DFT. Note that a window function, e.g., Hanning window, may be applied in the DFT. The output of the DFT of $Q^{(k)}$, denoted as $\hat{Q}^{(k)}$, is an $N_{node} \times N_{DFT}$ matrix of complex numbers

$$\hat{Q}^{(k)} = \begin{bmatrix} \hat{q}_1^{(k)} & \hat{q}_2^{(k)} & \cdots & \hat{q}_m^{(k)} & \cdots & \hat{q}_{N_{DFT}}^{(k)} \end{bmatrix} \tag{4}$$

where $\hat{Q}^{(k)} \in \mathbb{C}^{N_{node} \times N_{DFT}}$, $\hat{q}_m^{(k)} \in \mathbb{C}^{N_{node}}$, $m = 1, 2, \ldots, N_{DFT}$. $\mathbb{C}$ is the set of complex numbers.

The m-th column of the matrix $\hat{Q}^{(k)}$, denoted as $\hat{q}_m^{(k)}$ in Eq. (4), gives the frequency components of the uPSP measurements in the k-th block on the grid nodes at the frequency f_m, which is determined as

$$f_m = (m-1) \cdot f_{binWidth} \tag{5}$$

where $f_{binWidth}$ is the bin width of DFT, showing the frequency resolution. $f_{binWidth}$ is computed from the length of DFT, N_{DFT}, and the sample frequency of the uPSP measurements, f_{sample}, as shown below

$$f_{binWidth} = f_{sample} / N_{DFT} \tag{6}$$

B. Eigendecomposition of the Estimated CSD Matrix

In the second step of SPOD, the SPOD modes are determined from the eigendecomposition of the estimated CSD matrix at each frequency.

A matrix of the frequency components of the uPSP measurements in all blocks on the grid nodes at the frequency f_m, denoted as $\hat{X}_m$, is defined below

$$\hat{X}_m = \begin{bmatrix} \hat{q}_m^{(1)} & \hat{q}_m^{(2)} & \cdots & \hat{q}_m^{(k)} & \cdots & \hat{q}_m^{(N_{block})} \end{bmatrix} \tag{7}$$

where $\hat{X}_m \in \mathbb{C}^{N_{node} \times N_{block}}$, $\hat{q}_m^{(k)}$ is the m-th column of the matrix $\hat{Q}^{(k)}$ in Eq. (4), $k = 1, 2, \ldots, N_{block}$, $m = 1, 2, \ldots, N_{DFT}$. The CSD matrix at the frequency f_m is estimated from the matrix $\hat{X}_m$ with Welch's method, as shown below

$$\hat{C}_m = (1/N_{block}) \cdot \hat{X}_m \hat{X}_m^* = (1/N_{block}) \cdot \sum_{k=1}^{N_{block}} \left[\hat{q}_m^{(k)}\right] \left[\hat{q}_m^{(k)}\right]^* \tag{8}$$

where $\hat{C}_m \in \mathbb{C}^{N_{node} \times N_{node}}$ and $(\cdot)^*$ denotes the conjugate transpose.

The SPOD modes at the frequency f_m are determined as the eigenvectors of the estimated CSD matrix $\hat{C}_m$ and ranked in the descending order of the corresponding eigenvalues. Let N_{mode} be the number of SPOD modes, we have

$$\hat{C}_m \hat{\Phi}_m = \hat{\Phi}_m \Lambda_m \tag{9}$$

where

$$\hat{\Phi}_m = \begin{bmatrix} \hat{\phi}_{m,1} & \hat{\phi}_{m,2} & \cdots & \hat{\phi}_{m,i} & \cdots & \hat{\phi}_{m,N_{mode}} \end{bmatrix} \tag{10}$$

$$\Lambda_m = \begin{bmatrix} \lambda_{m,1} & & & & & \\ & \lambda_{m,2} & & & & \\ & & \ddots & & & \\ & & & \lambda_{m,i} & & \\ & & & & \ddots & \\ & & & & & \lambda_{m,N_{mode}} \end{bmatrix} \tag{11}$$

and

$$\lambda_{m,1} \geq \lambda_{m,2} \geq \cdots \geq \lambda_{m,i} \geq \cdots \geq \lambda_{m,N_{mode}} \geq 0 \tag{12}$$

In Eqs. (9)-(12), $\widehat{\Phi}_m \in \mathbb{C}^{N_{node} \times N_{mode}}$, $\hat{\phi}_{m,i} \in \mathbb{C}^{N_{node}}$, $\Lambda_m \in \mathbb{R}^{N_{mode} \times N_{mode}}$, $i = 1, 2, \ldots, N_{mode}$.

Note that $\hat{C}_m$ defined in Eq. (8) is a Hermitian matrix. Since the SPOD modes $\hat{\phi}_{m,i}$, $i = 1, 2, \ldots, N_{mode}$ are normalized, we have

$$\widehat{\Phi}_m^* \widehat{\Phi}_m = I_{N_{mode} \times N_{mode}} \tag{13}$$

where $I_{N_{mode} \times N_{mode}}$ is the identity matrix of the dimension $N_{mode} \times N_{mode}$. Eq. (13) shows the orthogonality of SPOD modes at a frequency. The estimated CSD matrix $\hat{C}_m$ at the frequency f_m can be represented by its eigenvectors and eigenvalues, as shown below

$$\hat{C}_m = \sum_{i=1}^{N_{mode}} \lambda_{m,i} \hat{\phi}_{m,i} \hat{\phi}_{m,i}^* \tag{14}$$

Eq. (14) shows that the eigenvalue of the estimated CSD matrix at a frequency gives the energy of the corresponding eigenvector, i.e., the SPOD mode, at the frequency.

C. A Computational Shortcut

Since the number of grid nodes, N_{node}, is much larger than the number of blocks, N_{block}, a computational shortcut is taken to compute the eigenvectors and eigenvalues of the estimated CSD matrix $\hat{C}_m$ defined in Eq. (8).

First, an $N_{block} \times N_{block}$ Hermitian matrix is defined below from the matrix $\hat{X}_m$

$$\widehat{M}_m = (1/N_{block}) \cdot \hat{X}_m^* \hat{X}_m \tag{15}$$

where $\widehat{M}_m \in \mathbb{C}^{N_{block} \times N_{block}}$. Then solve for the eigenvectors and eigenvalues of the matrix $\widehat{M}_m$, as shown below

$$\widehat{M}_m \widehat{\Psi}_m = \widehat{\Psi}_m \Lambda_m \tag{16}$$

where $\widehat{\Psi}_m \in \mathbb{C}^{N_{block} \times N_{mode}}$. Similar to Eq. (13), we have

$$\widehat{\Psi}_m^* \widehat{\Psi}_m = I_{N_{mode} \times N_{mode}} \tag{17}$$

Since $N_{node} \gg N_{block}$, the computation for the eigendecomposition of the matrix $\widehat{M}_m$ defined in Eq. (15) is much less than that for the eigendecomposition of the matrix $\hat{C}_m$ defined in Eq. (8). Finally, the eigenvectors of the estimated CSD matrix $\hat{C}_m$, i.e., the SPOD modes at the frequency f_m, are determined as

$$\widehat{\Phi}_m = \left(1/\sqrt{N_{block}}\right) \cdot \hat{X}_m \widehat{\Psi}_m \Lambda_m^{-1/2} \tag{18}$$

III. SPOD of uPSP Measurements in the uPSP LVDT

In this section, the outputs of SPOD of the uPSP measurements in the tests of a Mach sweep run of the uPSP LVDT are presented and discussed. The freestream Mach numbers of the tests were 0.70, 0.75, 0.80, …, and 1.20. The angle of attack and the angle of sideslip were both set to zero degrees in the tests.

A. Parameters of SPOD of uPSP Measurements

Table 1 shows parameters of SPOD of uPSP measurements in the tests of the Mach sweep run of the uPSP LVDT. As shown in the table, the timeseries of the uPSP measurements on 633,743 grid nodes were used to generate the SPOD outputs. The full timeseries of uPSP measurements were partitioned into overlapping blocks. There were 4,096 frames in each block and 2,048 frames overlapped, therefore, 13 blocks were generated from total number of 28,672 (which is equal to 4,096 × 7) frames.

The number of SPOD modes, N_{mode}, is determined by the rank of matrix $\hat{X}_m$ defined in Eq. (7), which again is limited by the number of grid nodes, N_{node}, and the number of blocks, N_{block}. Since $N_{node} \gg N_{block}$, we have $N_{mode} = N_{block} = 13$, as shown in Table 1.

Note that a Hanning window was applied in DFT of the uPSP measurements in each block and a uniform weighting function was used to process the data on the grid nodes. The sample frequency $f_{sample} = 10{,}000\ Hz$. For the SPOD outputs presented in this section, the frequency resolution, i.e., the bin width of DFT, $f_{binWidth} = 10{,}000\ Hz/4{,}096 = 2.44\ Hz$.

Table 1 Parameters of SPOD of the uPSP measurements in the tests of the Mach sweep run of the uPSP LVDT

Parameter	Value
Spectral Type	one-sided (real-valued signal)
Number of Grid Nodes, N_{node}	633,743
Number of Total Frames, N_{frame}	28,672
Number of Frames per Block, N_{DFT}	4,096
Number of Overlapped Frames, $N_{overlap}$	2,048
Number of Blocks, N_{block}	13
Number of SPOD Modes, N_{mode}	13
Windowing Function (time)	Hanning window
Weighting Function (space)	uniform
Sample Frequency (Hz), f_{sample}	10,000
Frequency Resolution (Hz), $f_{binWidth}$	2.44

B. SPOD Modes of uPSP Measurements in a Test at Mach Number 1.00

As examples, we present the SPOD modes of the uPSP measurements in a test of the Mach sweep run at Mach number 1.00. Fig. 3 shows the Sound Pressure Level (SPL, unit: dB, reference: 20 μPa) of the SPOD modes of the uPSP measurements of the test as the function of frequency (unit: Hz, in logarithmic scale), in the frequency band which we are interested in. In the figure, the SPLs of the 1st, 2nd, 3rd and 4th SPOD modes are illustrated in red, blue, magenta and cyan lines, respectively. The black line shows the SPL of all 13 SPOD modes of the uPSP measurements.

One specific frequency is selected as the reference, which is illustrated in a red dash line in Fig. 3. The results of the 1st, 2nd, 3rd and 4th SPOD modes at the reference frequency are presented below.

Figs. 4(a1-a4, b1-b4) show the magnitudes and phases of the 1st, 2nd, 3rd and 4th SPOD modes of the uPSP measurements at the reference frequency in the test at Mach number 1.00, plotted in a plane of x-coordinate and azimuth angle of the grid nodes. The SPOD modes are nondimensional, so are their magnitudes. The phase of the SPOD modes ranges from -180° to +180°. The grid nodes with the phase close to -180° are plotted in blue and the grid nodes with the phase close to +180° are plotted in yellow. In Figs. 5(a1-a4, b1-b4), the real and imaginary parts of the 1st, 2nd, 3rd and 4th SPOD modes at the reference frequency in the test at Mach number 1.00 are visualized on the surface of the scale model. In Figs. 4 and 5, the pressure variations due to the flows separated by the abort motor nozzles on the surface of the LAS, MPCV, USA and the Core Stage as well as the shock oscillations around the MPCV and the Core Stage flanges can be observed.

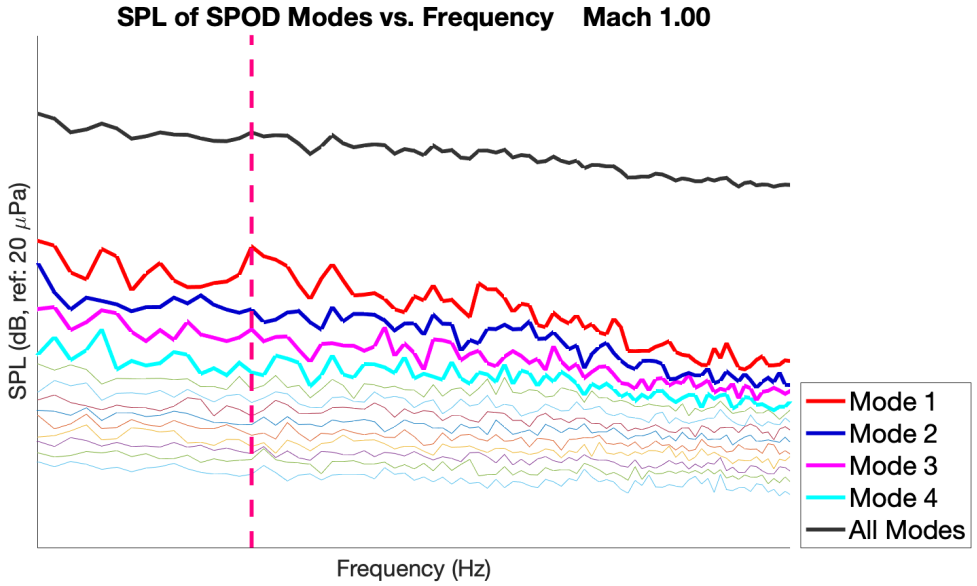

Fig. 3 SPL of the SPOD modes of the uPSP measurements in the test at Mach number 1.00 as the function of frequency.

Fig. 6 shows percentage of the energy (unit: psi^2) of the 1st, 2nd, 3rd and 4th SPOD modes in the energy (unit: psi^2) of all 13 SPOD modes in the test at Mach number 1.00 as the function of frequency (unit: Hz, in logarithmic scale), in the interested frequency band, which is the same as in Fig. 3. The reference frequency is also illustrated as a red dash line in Fig. 6. Table 2 shows percentage of the energy of the 1st, 2nd, 3rd and 4th SPOD modes in the energy of all 13 SPOD modes at the reference frequency and in the interested frequency band in the test at Mach number 1.00. As shown in the table, the 1st SPOD mode occupies 29.2% of the energy of all SPOD modes at the reference frequency and 19.8% of the energy of all SPOD modes in the interested frequency band. The 1st, 2nd, 3rd and 4th SPOD modes occupy 63.6% of the energy of all SPOD modes in total at the reference frequency and 54.9% of the energy of all SPOD modes in total in the interested frequency band.

C. 1st SPOD Modes of uPSP Measurements in the Tests at Mach Numbers 0.70 – 1.20

Now we present the 1st SPOD modes of the uPSP measurements of the Mach sweep run tests, at Mach numbers 0.70, 0.75, 0.80, …, and 1.20, and discuss the variations of the characteristics of the 1st SPOD modes as Mach number increases.

Fig. 7 shows the SPL (unit: dB, reference: 20 μPa) of the 1st SPOD modes of the uPSP measurements of the Mach sweep run tests, at Mach numbers 0.70, 0.75, 0.80, …, and 1.20, as the function of frequency (unit: Hz, in logarithmic scale), in the interested frequency band, which is the same as in Fig. 3. The range of the SPL axis in Fig. 7 is also the same as that in Fig. 3. It is seen from Fig. 7 that, as Mach number increases from 0.70 to 1.20, the SPL increases first, reaches the peak around Mach number 1.00, and then decreases. The same trend can also be observed in Fig. 8, which shows the SPL of the 1st SPOD modes of the uPSP measurements in the interested frequency band as the function of Mach number. The results of the 1st SPOD modes of the uPSP measurements at Mach numbers with high SPLs are presented below.

Figs. 9(a1-a4, b1-b4) show the magnitudes and phases of the 1st SPOD modes of the uPSP measurements at the reference frequency in the tests at Mach numbers 0.95, 1.00, 1.05 and 1.10, plotted in the plane of x-coordinate and azimuth angle of the grid nodes. In Figs. 10(a1-a4, b1-b4), the real and imaginary parts of the 1st SPOD modes of the uPSP measurements at the reference frequency in the same tests as in Figs. 9(a1-a4, b1-b4) are visualized on the surface of the scale model. In addition to the pressure variations due to the separated flows and the shock oscillations around the MPCV and the Core Stage flanges, which are observed in Figs. 4 and 5, it is also observed in Figs. 9 and 10 that the shock foot on the MPCV moves in the direction of the flow as Mach number increases.

IV. Conclusions

In this paper, we present preliminary results of SPOD of the uPSP measurements in the uPSP LVDT and demonstrate how the SPOD outputs can be used in the data visualization and analysis in the wind tunnel test. In Ref. [23], we discussed DMD of the uPSP measurements, which were collected in the Ascent Transient Aerodynamics Test (ATAT) of the SLS Block 1 cargo vehicle with the 11-by 11-foot Transonic Wind Tunnel at NASA Ames Research Center in September 2019. In the implementation of DMD, the mean was subtracted from the uPSP measurement, and the Fast Fourier Transform (FFT) was applied on the resulting data with zero mean to generate the DMD outputs. SPOD can be viewed as an extension of the DFT decomposition and the DMD. Our research shows that the combination of SPOD and DMD of uPSP measurements provides a powerful tool in the identification, diagnosis and analysis of the aerodynamic and aeroacoustic phenomena.

In Ref. [24], a new method for the diagnosis and analysis of the aeroacoustic phenomena is presented, based on the visualization and analysis of the DMD modes of the uPSP measurements. The wavelength of a traveling wave is conventionally estimated from the slope of the phase of the DMD mode versus the x-coordinate of the grid nodes along a streamline. The precision of the estimation of the wavelength is limited by the uncertainty of the phase of the DMD mode, which is mainly originated from the noise of the uPSP measurements. Since the SPOD modes are given by the linear combination, or weighted average, of DMD modes from all the partitioned blocks to yield uncorrelated modes that optimally capture the flow energy, the uncertainty of the phase of the SPOD mode is effectively reduced. Our research shows the precision of the estimation of the wavelength, as well as the corresponding propagation speed, of the travelling wave from the phase of the SPOD mode improves significantly, compared to the precision of the estimation from the phase of the DMD mode (Ref. [25]).

The SPOD modes of the uPSP measurements are determined in the frequency domain. The timeseries corresponding to each of the SPOD modes can be generated with the Inverse SPOD (Ref. [5]). The aerodynamic and aeroacoustic phenomena in the wind tunnel test usually lead to harmonic tones in the data collected in the test. Our research shows that the harmonic tones, e.g., the vortex shedding tone generated by the forward attachment of the Solid Rocket Booster (SRB), can be effectively separated from the broadband signals in the time domain with the Inverse SPOD of dominant SPOD modes of the uPSP measurements in the SLS ATAT. The outputs of the separation are used in the diagnosis and analysis of the aerodynamic and aeroacoustic phenomena as well as the generation of data products for the structural dynamics analysis (Ref. [26]).

What are presented in this paper are preliminary results. More research work on SPOD and DMD of the uPSP measurements in the wind tunnel tests will be done in the future.

Acknowledgment

The research work in this paper was funded by the NASA AETC Portfolio Office of ARMD. The authors would like to thank Evan Crowe, Avraham Gileadi and Sofia Tafolla for their expertise to support the uPSP LVDT, thank James Bell, Paul Bremner, Lawrence Hand, Rabindra Mehta, Blair Mclachlan, Jayanta Panda, James Ross and Nathanial Smith for their education and advice on the fluid mechanics and signal processing, thank Patrick Heaney, Jaffar Iqbal, Alan Landman, Bruce Laverde, David Piatak, James Ramey, Martin Sekula, Francesco Soranna, Thomas Steva, Craig Streett, Cory Wilbanks and Timothy Wray for their education and advice on the SLS, thank David Ellsworth, Christopher Henze, Patrick Moran, Bron Nelson and Timothy Sandstrom for their education and advice on the software development and parallel processing, and thank Max Amaya, Jennifer Baerny, Colin Davis, Maureen Delgado, Jennifer Everett, Ross Flach, Theodore Garbeff, James Prunty, Hannah Spooner, Tim Steiger, Michael Treece and Thomas Volden for their education and advice on the wind tunnel test. The authors also thank the SLS team for the preparation of the scale mode and the UPWT instrumentation and operation team of NASA Ames Research Center for the support of the uPSP LVDT.

References

[1] Lash, E. L., Murakami, D. D., Shaw-Lecerf, M. A., Lyons, K. R., Li, J., Califano, N. W., Crowe, E. and Roozeboom, N. H., "uPSP Launch Vehicle Demonstration Test at NASA Ames Research Center", AIAA SciTech Forum, Orlando, FL, January 2025.

[2] Powell, J. M., Murman, S. M., Ngo, C. L., Roozeboom, N. H., Murakami, D. D., Baerny, J. K., and Li, J., "Development of Unsteady-PSP Data Processing and Analysis Tools for the NASA Ames Unitary 11ft Wind Tunnel", AIAA Paper 2020-0292, AIAA SciTech Forum, Orlando, FL, January 2020.

[3] Towne, A., Schmidt, O. T. and Colonius, T., "Spectral Proper Orthogonal Decomposition and Its Relationship to Dynamic Mode Decomposition and Resolvent Analysis", *Journal of Fluid Mechanics*, Vol. 847, pp. 821-867, 2018.

[4] Schmidt, O. T. and Colonius, T., "Guide to Spectral Proper Orthogonal Decomposition", *AIAA Journal*, Vol. 58, No. 3, pp. 1023-1033, 2020.

[5] Nekkanti, A. and Schmidt, O. T., Frequency-Time Analysis, Low-Rank Reconstruction and Denoising of Turbulent Flows using SPOD", *Journal of Fluid Mechanics*, Vol. 926, A26, 2021.

[6] Schmid, P.J., "Dynamic Mode Decomposition of Numerical and Experimental Data", *Journal of Fluid Mechanics*, Vol.656, Aug. 2010, pp.5-28.

[7] Taira, K., Brunton, S.L., Dawson, S. T. M., Rowley, C.W., Colonius, T., McKeon, B.J., Schmidt, O.T., Gordeyev, S., Theofilis, V., and Ukeiley, L.S., "Modal Analysis of Fluid Flows: An Overview", *AIAA Journal*, Vol.55, No.12, 2017, pp.4013-4041.

[8] Rowley, C.W., Mezić, I., Bagheri, S., Schlatter, P., and Henningson, D. S., "Spectral Analysis of Nonlinear Flows", *Journal of Fluid Mechanics*, Vol. 641, No. 1, 2009, pp. 115–127.

[9] Chen, K. K., Tu, J. H., and Rowley, C.W., "Variants of Dynamic Mode Decomposition: Boundary Condition, Koopman, and Fourier Analyses," *Journal of Nonlinear Science*, Vol. 22, No. 6, 2012, pp. 887–915.

[10] "Pleiades Supercomputer", https://www.nas.nasa.gov/hecc/resources/pleiades.html. Accessed: 11/08/2024.

[11] "Spectral Proper Orthogonal Decomposition (SPOD)", https://www.mathworks.com/matlabcentral/fileexchange/65683-spectral-proper-orthogonal-decomposition-spod. Accessed: 11/08/2024.

[12] Mengaldo, G. and Maulik, R., "PySPOD: A Python package for Spectral Proper Orthogonal Decomposition (SPOD)", *Journal of Open Source Software*, 6(60), 2862, 2021.

[13] Schuster, D. M., Panda, J., Ross, J. C., Roozeboom, N. H., Burnside, N., Ngo, C. L., Kumagai, H., Sellers, M. E., Powell, J. M., Sekula, M. K., and Piatak, D. J., "Investigation of Unsteady Pressure-Sensitive Paint (uPSP) and a Dynamic Loads Balance to Predict Launch Vehicle Buffet Environments", NESC Report TI-14-00962, 2016.

[14] Roozeboom, N. H., Diosady, L. T., Murman, S. M., Burnside, N. J., Panda, J., and Ross, J. C., "Unsteady PSP Measurements on a Flat Plate Subject to Vortex Shedding from a Rectangular Prism", AIAA Paper 2016-2017, 54th AIAA Aerospace Sciences Meeting, San Diego, CA, January 2016.

[15] Panda, J., "Experimental Verification of Buffet Calculation Procedure Using Unsteady Pressure-Sensitive Paint", *Journal of Aircraft*, Vol.54, No. 5, 2017, pp. 1791-1801.
[16] Sellers, M. E., Nelson, M. A., Roozeboom, N. H., and Burnside, N. J., "Evaluation of Unsteady Pressure Sensitive Paint Measurement Technique for Space Launch Vehicle Buffet Determination", AIAA Paper 2017-1402, 55th AIAA Aerospace Sciences Meeting, Grapevine, TX, January 2017.
[17] Roozeboom, N. H., Ngo, C. L., Powell, J. M., Murakami, D. D., Ross, J. C., Murman, S. M., and Baerny, J. K., "Data Processing Methods for Unsteady Pressure-Sensitive Paint Application", AIAA 2018-1031, 56th AIAA Aerospace Sciences Meeting, Kissimmee, Florida, January 2018.
[18] Panda, J., Roozeboom, N.H., and Ross, J. C., "Wavenumber-Frequency Spectra on a Launch Vehicle Model Measured via Unsteady Pressure-Sensitive Paint", *AIAA Journal*, Vol. 57, No. 5, 2019, pp. 1801-1817.
[19] Roozeboom, N. H., Powell, J. M., Baerny, J. K., Murakami, D. D., Ngo, C. L., Garbeff, T. J., Ross, J. C., and Flach, R. L., "Development of Unsteady Pressure-Sensitive Paint Application on NASA Space Launch System", AIAA Paper 2019-3502, AIAA Aviation Forum, Dallas, TX, June 2019.
[20] Roozeboom, N. H., Murakami, D. D., Li, J., Powell, J. M., Baerny, J. K., Stremel, P. M., Volden, T. R., Flach, R. L., Douthitt, A. N., Steva, T. B., Ross, J. C., and Bell, J. H., "Recent Developments in NASA's Unsteady Pressure-Sensitive Paint Capability", AIAA Paper 2020-0516, AIAA SciTech Forum, Orlando, FL, January 2020.
[21] Roozeboom, N., Murakami, D., Li, J., Shaw-Lecerf, M., Lash, E.L, Califano, N., Stremel, P., Lyons, K., Baerny, J., Barreras, C., Ortega, J., Kato, K., Hand, L. and McLachlan, B., "NASA's Unsteady Pressure-Sensitive Paint Research and Operational Capability Developments", AIAA Paper 2023-0636, AIAA SciTech Forum, National Harbor, MD & Virtual, January 2023.
[22] Lash, E.L, Roozeboom, N. H., Murakami, D. D., Shaw-Lecerf, M. A., Li, J., Califano, N. W., Lyons, K. R., Stremel, P. M., Baerny, J., Barreras, C. E., Ortega, J. and Hand, L. A., "NASA's Unsteady Pressure-Sensitive Paint Phase I Development Overview", AIAA Paper 2024-0880, AIAA SciTech Forum, Orlando, FL, January 2024.
[23] Li, J., Lash, E. L., Roozeboom, N. H., Garbeff, T. J., Henze, C. E., Murakami, D. D., Smith, N. T., Baerny, J. K., Hand, L. A., Shaw-Lecerf, M. A., Stremel, P. M., and Tang, L. Z., "Dynamic Mode Decomposition of Unsteady Pressure-Sensitive Paint Measurements for the NASA Unitary Plan Wind Tunnel Tests", AIAA Paper 2022-0141, AIAA SciTech Forum, San Diego, CA & Virtual, January 2022.
[24] Li, J., Roozeboom, N. H., Lash, E. L., Shaw-Lecerf, M. A., Baerny, J. K., Garbeff, T. J., Hand, L. A., Henze, C. E., Murakami, D. D., and Smith, N. T., "Aeroacoustic Analysis using Dynamic Mode Decomposition of Unsteady Pressure-Sensitive Paint Measurements", AIAA Paper 2024-0882, AIAA SciTech Forum, Orlando, FL, January 2024.
[25] Li, J., "Spectral Proper Orthogonal Decomposition of uPSP Measurements in the SLS ATAT", Internal presentation at NESC Load and Dynamics Team Meeting, Virtual, November 2023.
[26] Li, J., "Spectral Proper Orthogonal Decomposition of uPSP Measurements and its Application in Structral Dynamics Analysis", Internal presentation at NESC Load and Dynamics Team Face-to-Face Meeting, Moffett Field, CA, May 2024.

1st SPOD Mode, Mach 1.00

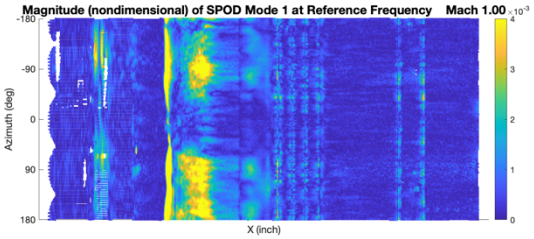

(a1)

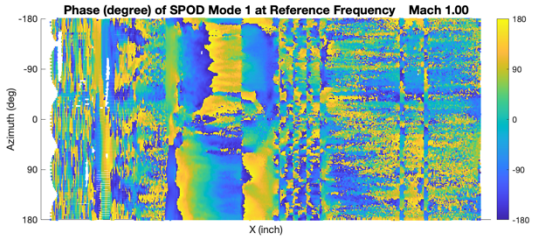

(b1)

2nd SPOD Mode, Mach 1.00

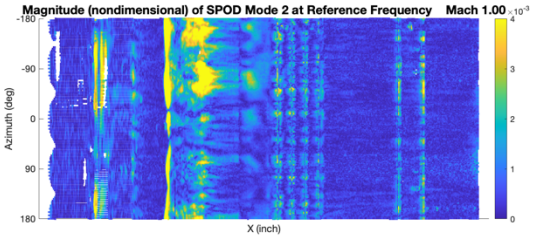

(a2)

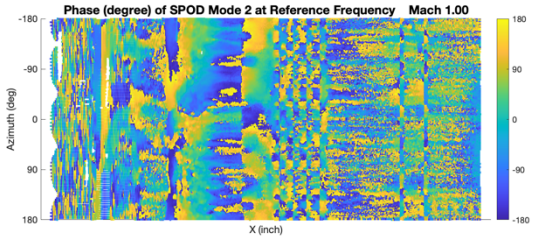

(b2)

3rd SPOD Mode, Mach 1.00

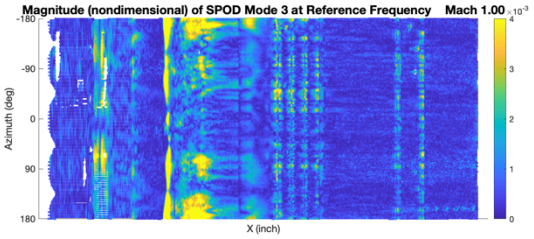

(a3)

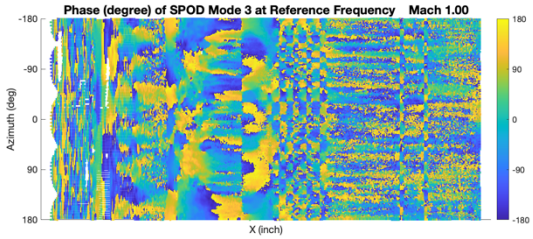

(b3)

4th SPOD Mode, Mach 1.00

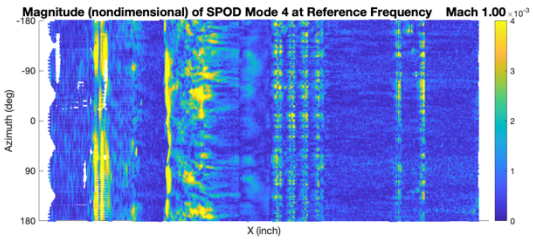

(a4)

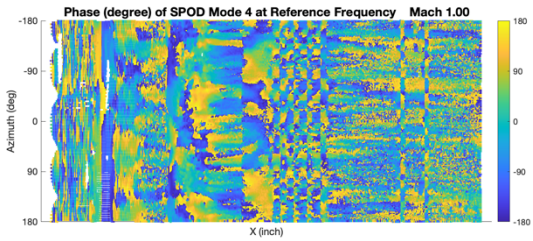

(b4)

Fig. 4 Magnitudes (a1-a4) and phases (b1-b4) of the 1st, 2nd, 3rd and 4th SPOD modes of the uPSP measurements at the reference frequency in the test at Mach number 1.00.

1st SPOD Mode, Mach 1.00

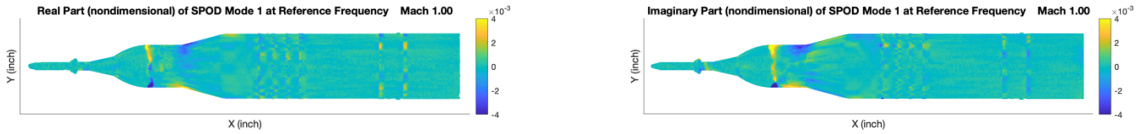

(a1) (b1)

2nd SPOD Mode, Mach 1.00

(a2) (b2)

3rd SPOD Mode, Mach 1.00

(a3) (b3)

4th SPOD Mode, Mach 1.00

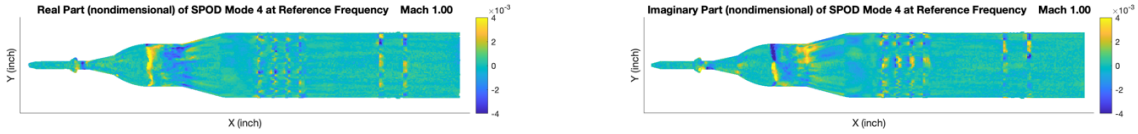

(a4) (b4)

Fig. 5 Real (a1-a4) and imaginary (b1-b4) parts of the 1st, 2nd, 3rd and 4th SPOD modes of the uPSP measurements at the reference frequency in the test at Mach number 1.00.

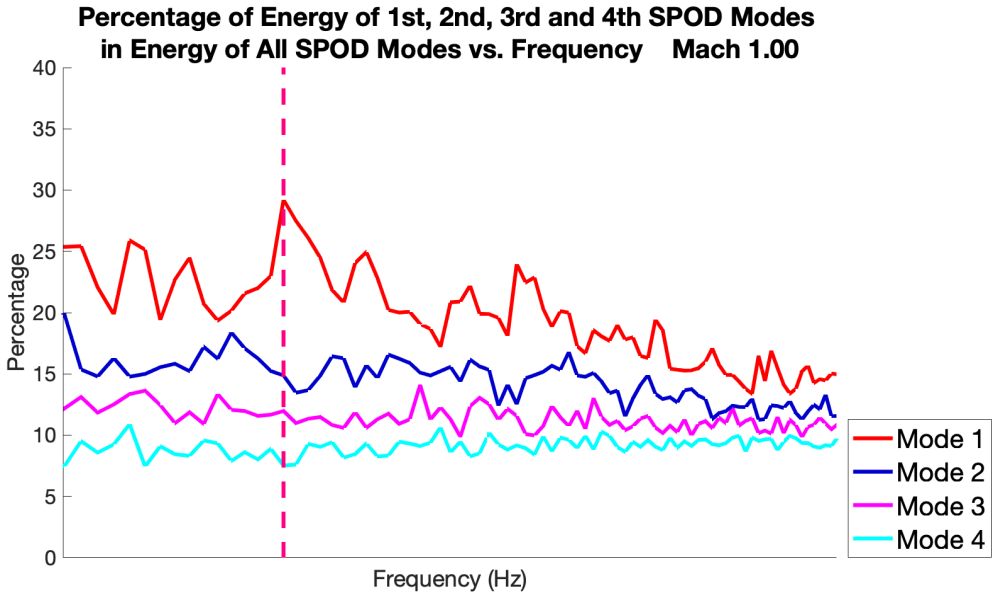

Fig. 6 Percentage of the energy of the 1st, 2nd, 3rd and 4th SPOD modes in the energy of all SPOD modes in the test at Mach number 1.00 as the function of frequency.

Table 2 Percentage of the energy of the 1st, 2nd, 3rd and 4th SPOD modes in the energy of all SPOD modes at the reference frequency and in the interested frequency band in the test at Mach number 1.00

SPOD Mode	Percentage of Energy of the SPOD Mode in Energy of All SPOD Modes	
	At Reference Frequency	In Interested Frequency Band
1st SPOD Mode	29.2%	19.8%
2nd SPOD Mode	14.9%	14.5%
3rd SPOD Mode	12.0%	11.5%
4th SPOD Mode	7.5%	9.1%
Sum	63.6%	54.9%

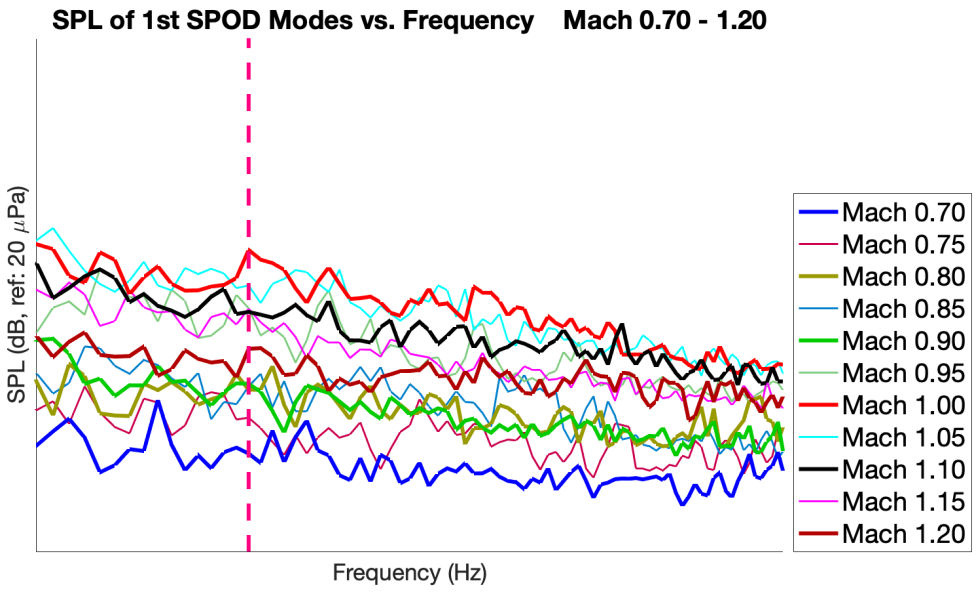

Fig. 7 SPL of the 1st SPOD modes of the uPSP measurements in the tests at Mach numbers 0.70, 0.75, 0.80, …, 1.20 as the function of frequency.

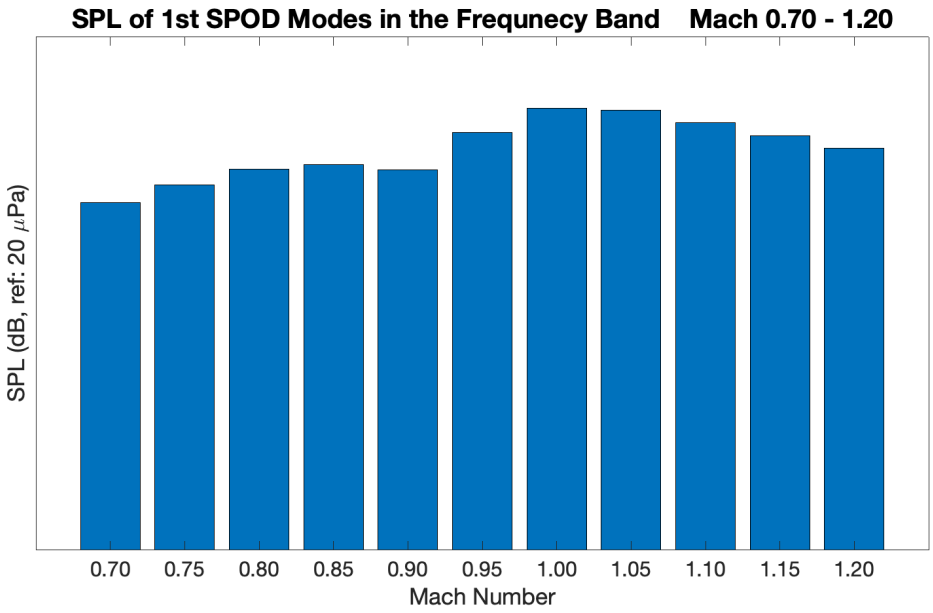

Fig. 8 SPL of the 1st SPOD modes of the uPSP measurements in the interested frequency band as the function of Mach number.

1st SPOD Mode, Mach 0.95

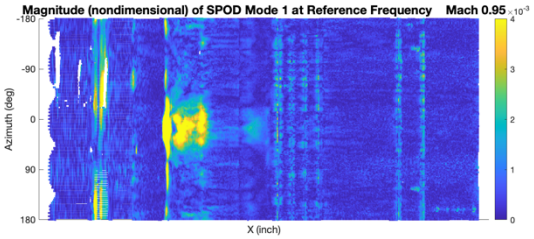

(a1)

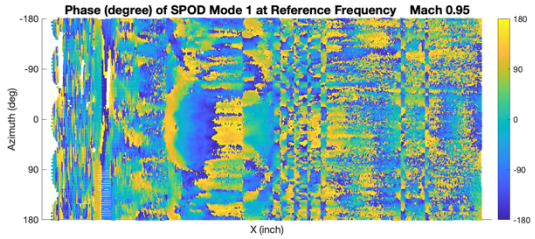

(b1)

1st SPOD Mode, Mach 1.00

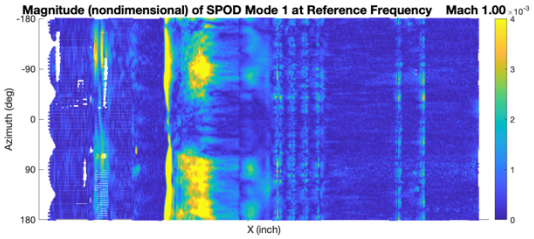

(a2)

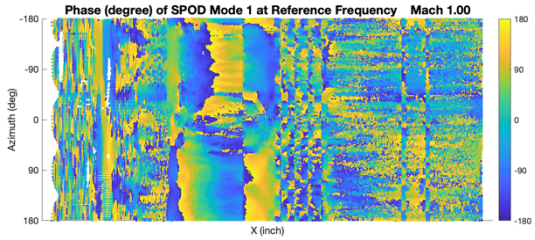

(b2)

1st SPOD Mode, Mach 1.05

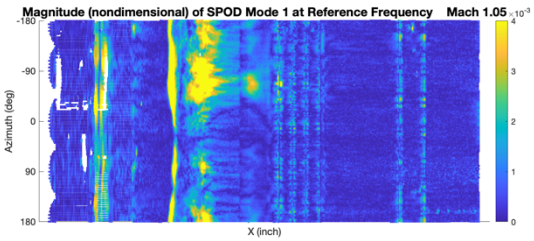

(a3)

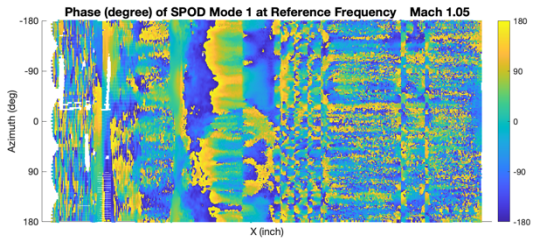

(b3)

1st SPOD Mode, Mach 1.10

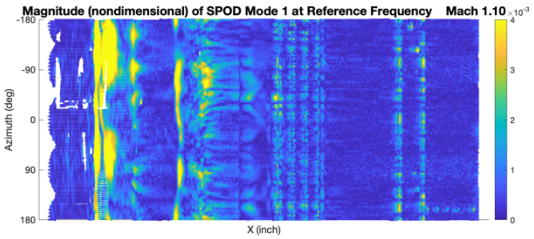

(a4)

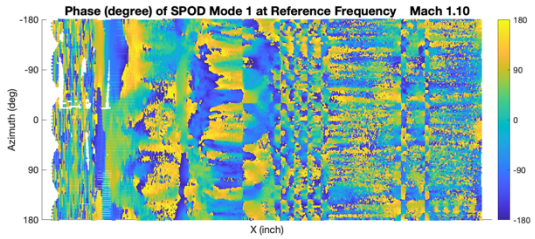

(b4)

Fig. 9 Magnitudes (a1-a4) and phases (b1-b4) of the 1st SPOD modes of the uPSP measurements at the reference frequency in the tests at Mach numbers 0.95, 1.00, 1.05 and 1.10.

1st SPOD Mode, Mach 0.95

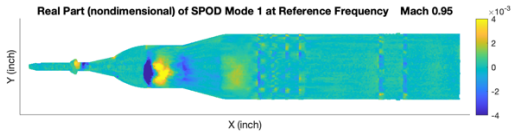

(a1)

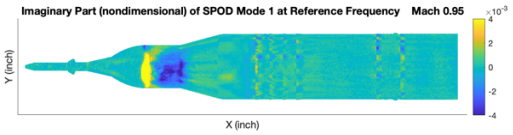

(b1)

1st SPOD Mode, Mach 1.00

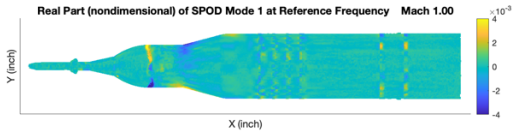

(a2)

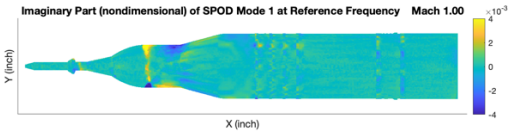

(b2)

1st SPOD Mode, Mach 1.05

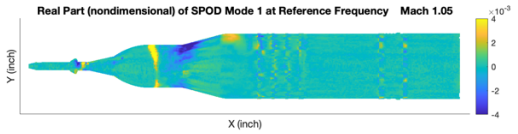

(a3)

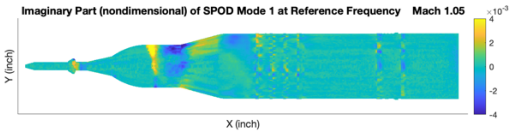

(b3)

1st SPOD Mode, Mach 1.10

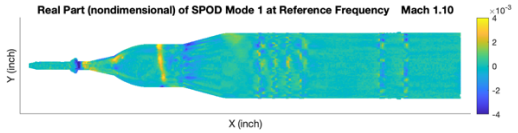

(a4)

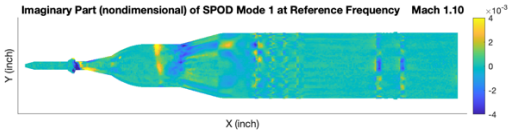

(b4)

Fig. 10 Real (a1-a4) and imaginary (b1-b4) parts of the 1st SPOD modes of the uPSP measurements at the reference frequency in the tests at Mach numbers 0.95, 1.00, 1.05 and 1.10.